Performance optimization of bilayer organic photovoltaic cells

MOSTAFA A. EL-AASSER
Physics Department, Faculty of Science, Ain Shams University, Abbassia, Cairo 11566, Egypt

In this paper ITO/P3HT/PCBM/Al Organic Photovoltaic Cells (OPVs) are simulated and their performance parameters are evaluated. The IV characteristics, carrier concentrations, and band diagram are simulated at different applied voltages. Performance optimization of the device dimensions and material parameters are carried out. Maximum power of 28.3 W/m^2, efficiency of 2.8, a fill factor of 0.7, V_{OC} of 0.66 V, and J_{SC} of 6 mA/cm^2 are obtained, assuming 1 kW/m^2 irradiance with AM 1.5 solar spectrum. When OPV is subjected to constant illumination, with 2×10^{22} cm^{-3}s^{-1} photons absorption rate in the active layer, the obtained performance parameters are 33.6 W/m^2, 3.4, 0.7, 0.7 V, and 7.3 mA/cm^2 for the maximum power, efficiency, fill factor, V_{OC}, and J_{SC} respectively.

(Received April 23, 2016; accepted September 29, 2016)

Keywords: Organic photovoltaic cells, Organic solar cells, Solar energy, Renewable energy, Energy harvesting

1. Introduction

Organic Photovoltaic cells (OPVs) have drawn increasing interest in recent decades making their way into the commercial world. OPVs are considered to be an alternative to their inorganic counterparts since organic materials are light in weight, flexible, and potentially less costly. In the last few years, organic solar cells (SCs) that are based on π-conjugated polymers (PCPs) have attracted so much interest in academia. PCPs are promising materials because of their versatility, flexibility, electronic properties, easy of processing, and low cost. Therefore Organic SCs promise to be able to provide a cost effective alternative to inorganic SCs. OPVs consist of hydrocarbon compounds, deposited as ultrathin layers (some tens of nm) on a substrate. Actually, the most efficient OPVs to date having effective power conversion (up to 9 % [1–3]) are based on bulk heterojunctions (BHJ) formed as a blend of a PCP and fullerene [4]. Despite the significant advances that have been achieved in device performance, the complexity of charge carrier photogeneration as well as the evolution in the donor–acceptor blends for OPV applications is nevertheless the focus of a lot of research seeking for developing novel organic SC devices with high power conversion efficiency [5, 6]. The organic semiconductors are composed of series of overlapping σ-orbitals formed via sp2 hybridization such that the π-electron is left unbounded. As a result, this creates a conjugated chain of delocalized π-electrons which produce a highly anisotropic quasi one-dimensional electronic structure. This structure is basically different from that of conventional inorganic semiconductors. The photo-excitations in PCPs result in large binding energy excitons (bound electron-hole pairs) rather than free charge carriers or small binding energy excitons as in inorganic semiconductors [7]. Excitons, the molecular excited states due to absorption of light, are strongly bound because of the weak interactions and low dielectric constant in a molecular solid.

The excitons have to be split into holes and electrons, which are subsequently collected at different electrodes. An effective dissociation of excitons is provided by a heterojunction of two molecules with different frontier orbital energies such that the electron is transferred to the acceptor and the hole remains on the donor molecule. This junction can be realized by two distinct layers forming a planar heterojunction. Electrodes are attached to collect the charges by providing an ohmic contact. The bilayer OPV device is shown in Fig. 1(a) with its heterojunction band diagram in Fig. 1(b). It consists mainly of two organic materials that are electron donating (donor) and electron accepting (acceptor) sandwiched between two conducting contacts. The conducting contacts such as indium tin oxide (ITO) is called anode while the lower work function metal is called cathode. Many metals are typically utilized for the non-transparent back contact such as Mg, Ca, or Al. The materials for the transparent front electrode are much more limited. ITO is the most prominent transparent electrode for OPV devices. ITO provides sufficiently high transmittance (~90%) and low sheet resistance (~10 Ω/sq). However, ITO is an expensive and brittle transparent conducting electrode. Replacing ITO with chemical vapor deposition (CVD) graphene could eliminate one of the drawbacks associated with OPVs. ZnO doped with group III elements (e.g. B [8], Ga [9-11] and Al [12, 13]) are alternative transparent electrode materials. Other approaches to replace ITO are carbon nanotubes [14], graphene [15], highly conductive polymers [16], metal grids [17], metal nano-meshes [18], and optically thin metal layers alone [19] or thin metals combined with other metal oxides [20].

OPVs can be classified by the type of donor-acceptor materials employed into polymer-fullerene, polymer-polymer, and hybrid OPVs. The polymers in OPVs are generally conjugated (alternating single and double bonded carbon) and possess delocalized (not associated with a single atom) electrons that can absorb photons. Polymers serve as the acceptor and donor materials; however, fullerenes- spherical, ellipsoidal, or tube-like carbon molecules are highly effective electron donors. Hybrid OPVs incorporate metal oxide nanoparticles into the organic active materials [21]. One of the most common and best performing OPVs is a polymer-fullerene cell with poly (3-hexylthiophene) (P3HT) as the donor and the fullerene [6,6]-phenyl-C61 butyric acid methyl ester (PCBM) as the acceptor [22, 23]. The most important feature in this structure type is that the charge generation is relatively independent of the bias voltage.

Several obstacles prevent OPVs to be mature business that capable of competing with the inorganic PVs. The cost of OPVs are still high (largely due to the costly manufacturing processes), the efficiency of OPVs need to be improved, the life time of OPVs are not long enough compared to their inorganic counterparts, and the physics models of the behavior of the devices are not completely satisfactory. All these limitations have invoked the demand for new organic materials, improved device architectures, and low-cost fabrication methods.

The analysis of planar bilayer heterojunction is the root of the research on OPVs because of its simplicity compared to the complex random morphologies which can be geometrically transformed to an equivalent planar structure. A small molecule device is considered that can be evaporated as a truly bilayer structure [24]. Achieving a better theoretical understanding of the physics of these devices is the motivation behind this work. Quantitative estimation of the effect of device dimensions and material parameters on the OPVs performance is presented. Researchers have tried to analyze the planar hetrojunction OPVs performance so far by making change in active layer materials, electrodes workfunction, recombination rate etc. Although the device dimensions have a huge impact on the performance of OPVs, it received less attention. Therefore, this paper focuses on the effect of dimensions as well as material parameters on the OPVs performance.

2. Device modeling

Most OPV devices consist of a transparent front electrode and a non-transparent reflecting back electrode. Light that enters the OPV cell through the transparent electrode is reflected at the non-transparent electrode. Therefore, the light passes the active layer twice and a standing wave is formed with null electric field strength at the reflecting electrode. The electric field maximum is somewhere in the bulk depending on the refractive index and the thicknesses of the layers. The absorption of light depends on its electric field strength which depends on the phase. For OPV cells with a photoactive layer thickness in the range of 100 nm, interference effects may become important. The absorbing active layer thickness needs to be correlated to the mobility-lifetime product of the photo-generated charge carriers within the active layer, so that most photo-generated charge carriers can reach the electrodes.

The OPV is exposed to ambient temperature 300 K, irradiance 1 kW/m^2, with AM 1.5 solar spectrum. Matrix method is one of the most elegant methods to describe the general multilayer structures. The photon absorption profile is calculated in each layer using this method [25]. Excitons, the tightly bound electron-hole pairs (neutral charge) which are created due to the photon absorption, move inside the active layer by diffusion according to the diffusion equation

$$D_{ex}\frac{d^2n_{ex}}{dx^2} = G_{ex}(x) - R_{ex}(x). \quad (1)$$

Where D_{ex} is the exciton diffusion coefficient, n_{ex} is the exciton concentration, G_{ex} and R_{ex} are the exciton generation and recombination rates, respectively. The exciton recombination rate is defined as $R_{ex}(x) = n_{ex}/t_{ex}$, where t_{ex} is the exciton lifetime. The exciton diffusion length, a distance that exciton can move without decay or recombination, is given by $L_{ex} = \sqrt{D_{ex}.t_{ex}}$. At the donor-acceptor heterojunction, the excitons dissociate into electrons and holes, therefore the exciton concentration is assumed to be zero at the heterojunction. The work function difference between the anode and cathode creates an electric field that drifts the holes to the donor and electrons to the acceptor. The charge carrier generation in OPVs is summarized in four processes; photon absorption, exciton diffusion, charge transfer, and charge transport and collection. Drift-diffusion transport of electrons and holes is given by the equations

$$J_e(x) = e\mu_e n(x)E(x) + eD_e\frac{dn(x)}{dx} \quad (2)$$

$$J_h(x) = e\mu_h h(x)E(x) - eD_h\frac{dh(x)}{dx} \quad (3)$$

where e is the electron charge, μ_e and μ_h are the electron and hole mobilities, $n(x)$ and $h(x)$ are the electron and hole concentrations, $E(x)$ is the electric field, D_e and D_h are the electron and hole diffusion coefficients, respectively. The Electric field $E(x)$ is calculated by solving Poisson equation self-consistently with the transport equations. The boundary conditions are

$$n(d) = n_{Al} = N_C exp\left(-\frac{\varphi_c - \chi_A}{kT}\right) \quad (4)$$

$$p(0) = p_{ITO} = N_V exp\left(-\frac{\varphi_a - \chi_D}{kT}\right). \quad (5)$$

Where φ_c is and φ_a are the workfunctions of cathode and anode, χ_A and χ_D are the LUMO level for acceptor and donor, N_C and N_V are the effective densities of conduction and valance bands. By solving the drift-diffusion based transport equations for the flow of excitons, electrons and holes, the IV curve is calculated.

Based on the IV characteristics, the OPV performance parameters namely, the efficiency (η), maximum power current density (J_m), short circuit current density (J_{SC}), fill factor (FF), maximum power voltage (V_m), open circuit voltage (V_{OC}) , and the maximum power density (P_m) are calculated. Where $P_m = V_m J_m$, $FF = \frac{P_m}{V_{OC} J_{SC}}$ and $\eta = \frac{P_m \times 100\%}{Irradiance}$. All optical parameters are obtained from [26-28]. The materials parameters used in simulation are summarized in Table 1.

Table 1. Materials parameters used for the simulation of OPV.

Material parameter	Default values
Hole mobility in donor, μ_h	0.0001 $cm^2/V.s$
Electron mobility in acceptor, μ_e	0.0005 $cm^2/V.s$
Exciton diffusion length in donor, L_{ex}^D	20 nm
Exciton diffusion length in acceptor, L_{ex}^A	5 nm
Bi-molecular recombination coefficient, γ	10^{-9} cm^3/s
Donor Lowest Unoccupied Molecular Orbital, DL (LUMO)	3 eV
Acceptor LUMO, AL	3.7 eV
Donor Highest Occupied Molecular Orbital (HOMO), DH	4.9 eV
Acceptor HOMO, AH	6.1 eV
Effective density of states at LUMO, N_L	10^{21} cm^{-3}
Effective density of states at HOMO, N_H	10^{21} cm^{-3}
Anode workfunction, φ_a	4.7 eV
Cathode workfunction, φ_c	3.9 eV

3. Simulation results

The simulation of dark and light IV characteristics is shown in Fig. 1 (c). It is a typical Solar cell IV graph. From this figure, the maximum power current density (J_m), maximum power voltage (V_m), maximum power (P_m), short circuit current density (J_{SC}), open circuit voltage (V_{OC}), and the fill factor (FF) can be easily calculated. In Fig. 1(d) the hole and electron concentrations versus position at voltages 0, 0.3, and 0.7 are shown. It is noted that the difference between hole and electron concentrations, at the donor-acceptor interface, go up by increasing the applied voltage. This is due to the decrease in the height of the band diagram. This variation in the band diagrams due to the change in voltages (0, 0.3, and 0.7) is shown in Fig. 1(e).

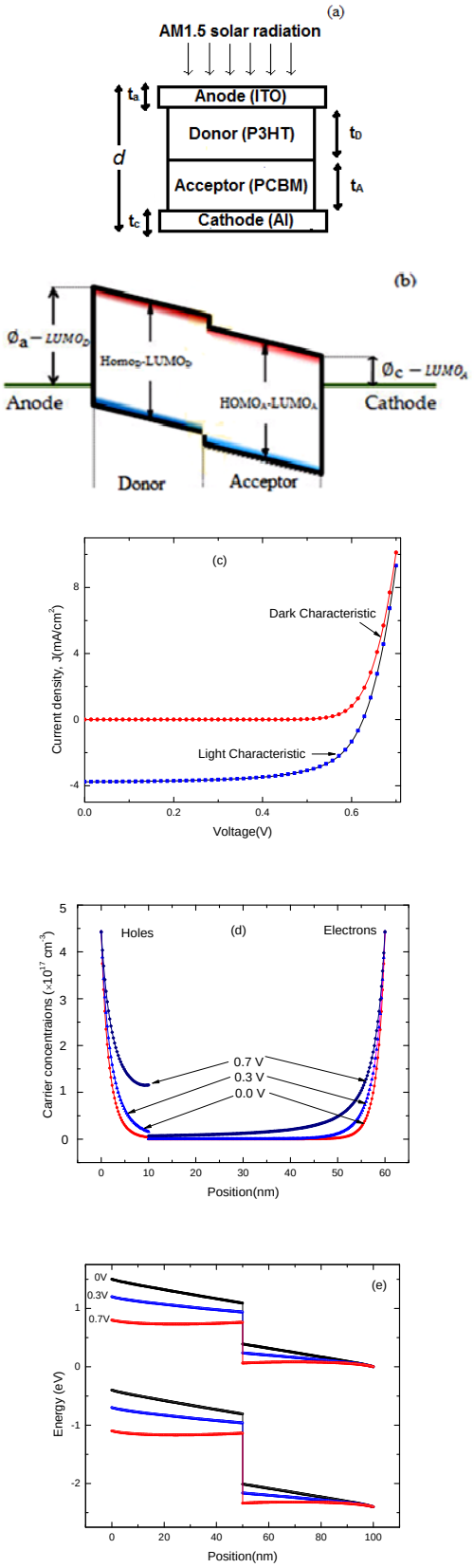

Fig. 1. (a) Schematic of planar heterojunction OPV. (b) Schematic of planar heterojunction band diagram. (c) IV characteristics. (d) Carrier concentrations versus position at voltages 0, 0.3, and 0.7. (e) Band diagrams versus position at voltages 0, 0.3, and 0.7V.

3.1.Device dimension effect on performance parameters

The effect of the device dimensions on the fill factor (FF), maximum power voltage (V_m), and open circuit voltage (V_{OC}) is studied. The maximum power (P_m) as a function of device dimensions is also investigated. The device dimensions are optimized for maximum performance in the following order: donor, acceptor, cathode, anode, and interface.

3.1.1. Donor thickness optimization

The optimization is carried out first for the donor thickness (t_D) as a variable while keeping the other dimensions fixed. Maximum magnitude of efficiency (η), maximum power current density (J_m), and short circuit current density (J_{SC}) were obtained at the dimensions t_D = 30 nm, as in Fig. 2(a), t_A = 50 nm, as in Fig. 3(a), t_c = 100 nm, as in Fig. 4(a), t_a = 120 nm, as in Fig. 5(a), and interface layer thickness = 0.5 nm, as in Fig. 5(b).

While keeping the other dimension parameters fixed the parameters η, J_m, and J_{SC} versus t_D, are shown in Fig. 2(a). Thicker donor absorbs more photons which gives higher η, J_m, and J_{SC} up to the peak at t_D = 30 nm. After that charge extraction gets difficult therefore η, J_m, and J_{SC} decrease. The parameters FF, V_m, and V_{OC} versus t_D, keeping the other dimensions fixed, are shown in Fig. 2(b). Since $FF = \frac{V_m J_m}{V_{OC} J_{SC}}$, it increases as the numerator supersedes denominator. FF and V_m maximum values are 0.71 and 0.51 at t_D = 20 nm while the V_{OC} is approximately ~ 0.63 V and then increasing slightly to be 0.64V. Since organic materials have poor mobilities, higher thickness leads to more recombination, hence fill factor gets lower. P_m as a function of donor thickness is shown in Fig. 2(c). The maximum P_m occurs also at t_D = 30 nm. Fig. 3(a) shows η, J_m, and J_{SC} versus acceptor layer thickness t_A, keeping the other dimension parameters fixed (t_D = 30 nm, Interface layer thickness = 1 nm, and t_a = t_c = 100 nm).

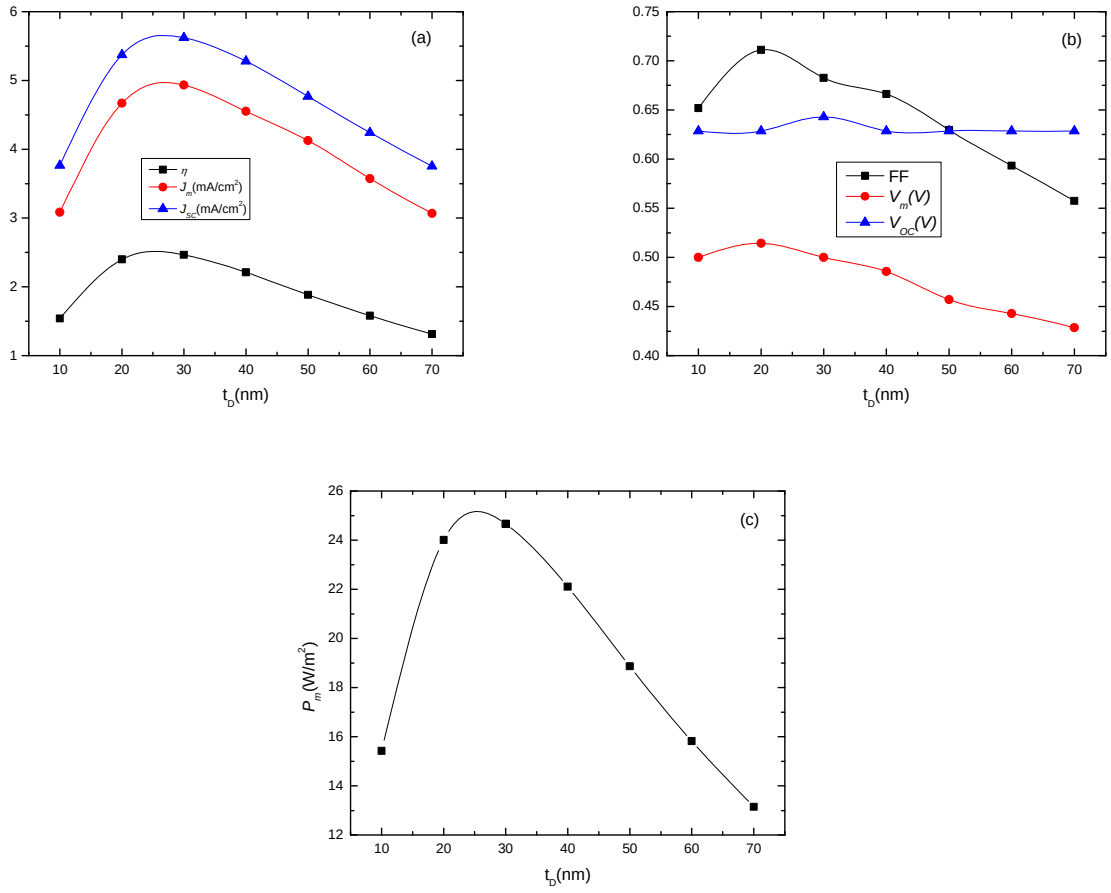

Fig. 2. (a) η, J_m, and J_{SC} versus t_D, (b) FF, V_m and V_{OC} versus t_D, (c) P_m versus t_D, t_A = 50 nm, interface thickness =1 nm, t_c = 100 nm, t_a = 100 nm.

3.1.2. Acceptor thickness optimization

The optimum values of η, J_m, and J_{SC} are 2.5, 4.8, 5.6 at t_A = 50 nm. Fig. 3(a), η, J_m, and J_{SC} curves as a function of t_A are smoother than those in Fig. 2(a) as a function of t_D. Therefore the acceptor effect on charge carriers is stronger than donor. In Fig. 3(b), the effect of t_A on FF, V_m and V_{OC} is shown. The maximum value of FF and V_m are 0.71 and 0.51 at t_A = 30 nm while V_{OC} takes its maximum value 0.62 at t_A = 50 nm. Fig. 3(c) depicts P_m versus t_A showing a maximum of 25 at t_A = 50 nm.

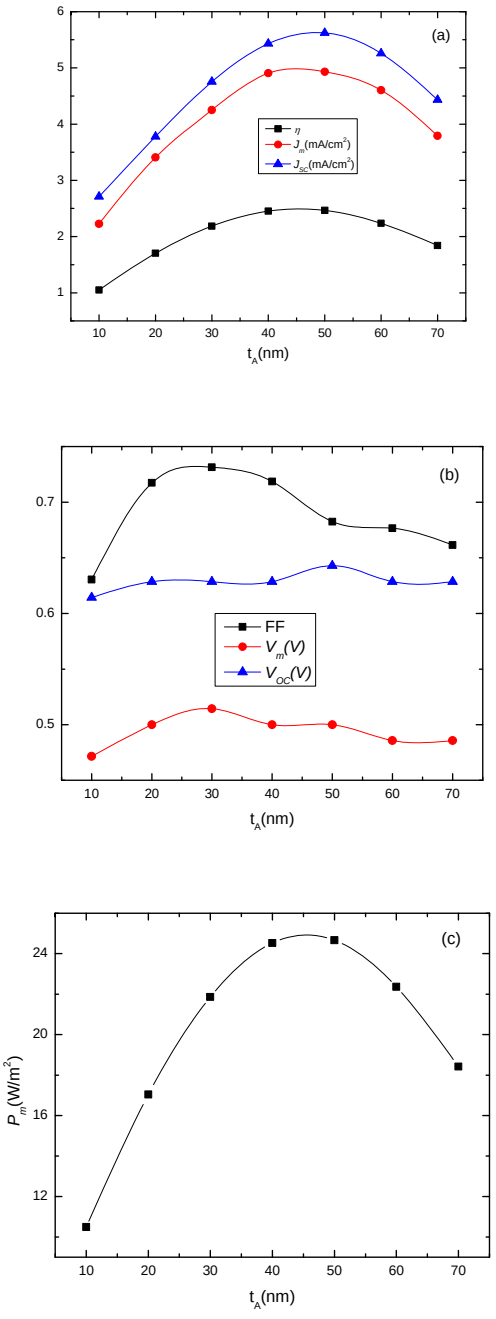

Fig. 3. (a) η, J_m, and J_{SC} versus t_A, (b) FF, V_m and V_{OC} versus t_A, (c) P_m versus t_A, t_D =30nm, interface layer=1 nm, t_c = 100 nm, t_a = 100 nm.

3.1.3. Cathode thickness optimization

The cathode thickness t_c affects slightly the performance parameters as shown in Fig. 4(a-c). Fig. 4(a) shows an increase in η, J_m, and J_{SC} at t_c = 20 to t_c = 40 nm then remain constant; this means that 40 nm cathode thickness is enough to collect the electrons. V_m is constant (saturation) at 0.5 V in Fig. 4(b), while V_{OC} slight increase corresponds to slight decrease in FF from 0.7 to 0.68. The saturation of P_m as a function of t_c is shown in Fig. 4(c). Ag and Al electrodes, either bare or coated, result in highest J_{SC} values in both conventional and inverted configurations [25, 26].

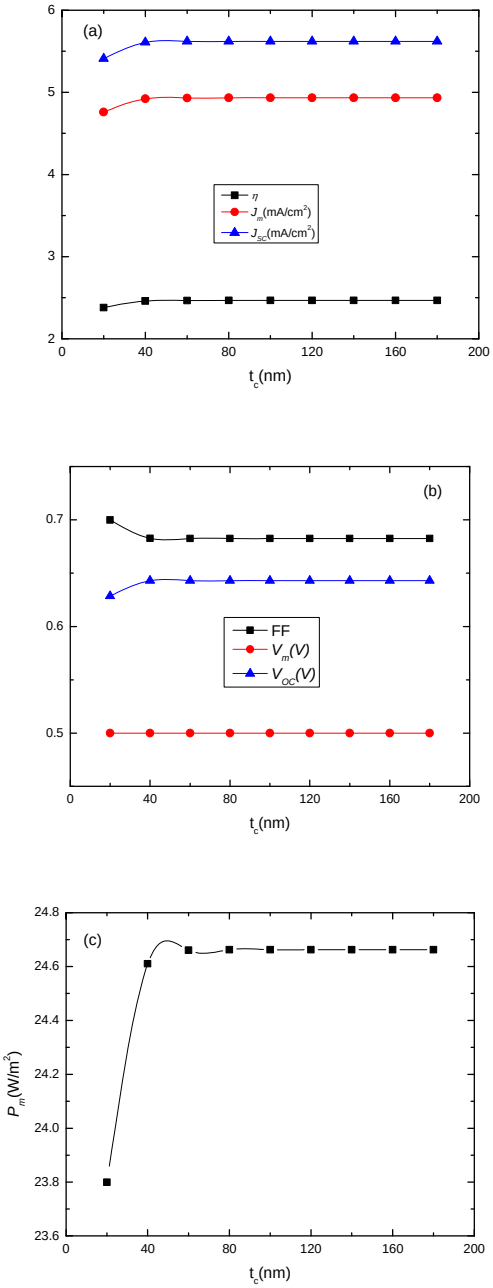

Fig. 4. (a) η, J_m, and J_{SC} versus t_c, (b) FF, V_m and V_{OC} versus t_c, (c) P_m versus t_c, t_D = 30 nm, t_A = 50 nm, interface thickness =1 nm, t_a = 100 nm.

3.1.4. Anode thickness optimization

When varying the anode thickness, an oscillatory-type behavior is observed in the performance parameters as shown in Fig. 5(a-c). This behavior could be due to the optical interference in the transparent anode (ITO). The highest η, J_m, and J_{SC} are obtained at $t_a \sim 130$ nm. In Fig. 5(b), V_m remains constant at 0.5 V. P_m has minimum value (~20.5 W/m^2) at t_a = 40 nm and maximum value (~26.2 W/m^2) at t_a = 120 nm as shown in Fig. 5(c).

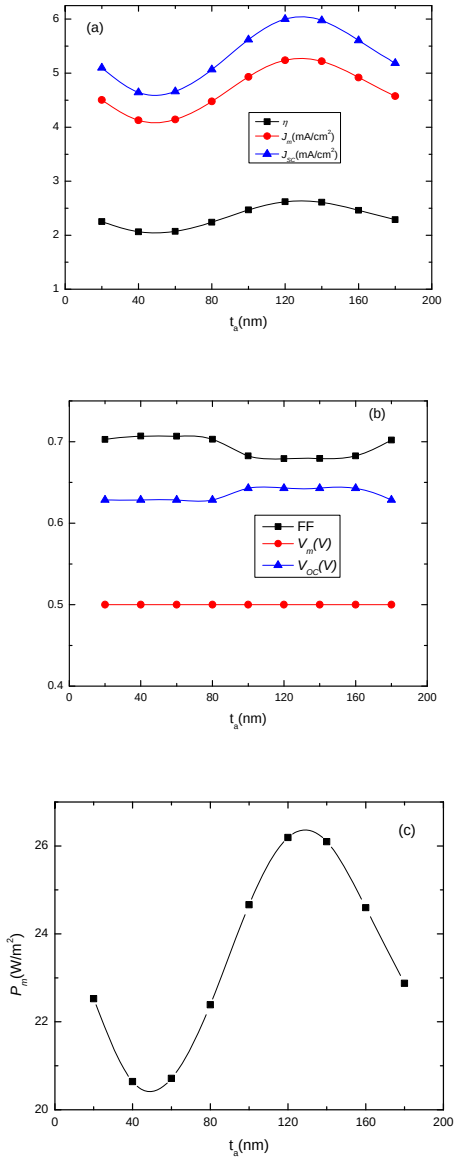

Fig. 5. (a) η, J_m, and J_{SC} versus t_a, (b) FF, V_m and V_{OC} versus t_a, (c) P_m versus t_a, t_A = 50 nm, t_D = 30 nm, interface thickness =1 nm, t_c = 100 nm.

Sharp interface (~1 nm roughness) in P3HT/PCBM bilayer was reported using a combination of AFM and optical measurements [22]. All performance parameters, efficiency, maximum power current density, short circuit current density, fill factor, maximum power voltage, open circuit voltage, and maximum power density are degraded by increasing the interface layer thickness. This is due to its negative effect on the charge carrier transport and exciton dissociation.

3.1.5. Interface thickness optimization

The interface layer thickness effect on the performance parameters is shown in Fig. 6(a-c). All parameters have shown a slight decrease with increasing the interface layer thickness. P_m gets lower from 28.2 to 24 W/m^2 as the interface layer thickness varies from 0.4 to 2 nm.

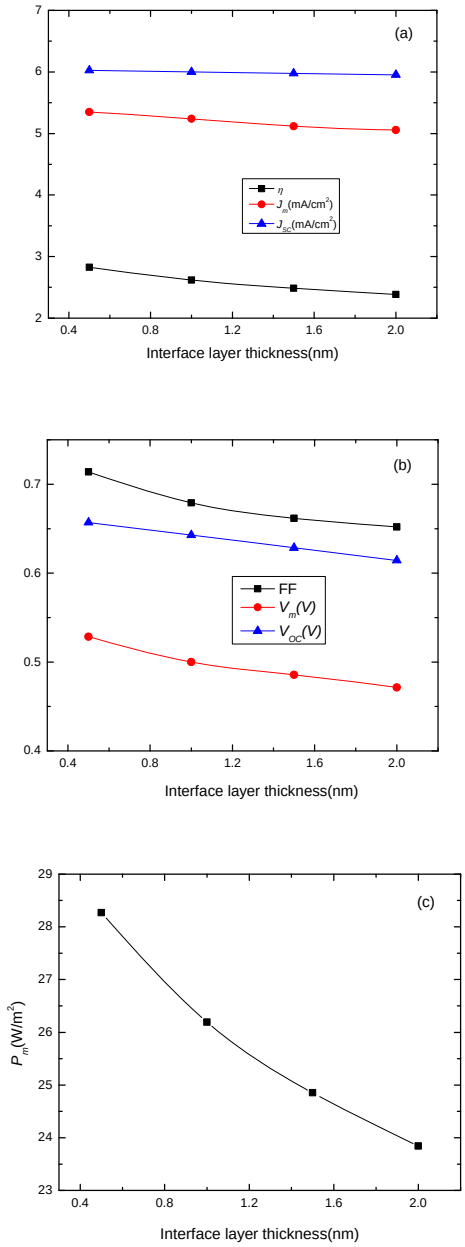

Fig. 6. (a) η, J_m, and J_{SC} versus Interface layer thickness, (b) FF, V_m and V_{OC} versus Interface layer thickness, (c) P_m versus Interface layer thickness, t_D =30nm, t_A = 50 nm, t_c = 100 nm, t_a = 120 nm.

3.2. Material effect on performance parameters

The parameters η, J_m, and J_{SC} increase with the increase in the electron mobility in acceptor (μ_e) then get saturated at 10^{-3}(cm^2 / V.s) as in Fig. 7(a). Fig. 7(b) shows a constant V_{OC} while FF and V_m increase with increasing value of μ_e until saturation is reached as from $\mu_e = 10^{-3}$(cm^2 / V.s). P_m shows the saturation at the same value as shown in Fig. 7(c). The effect of varying electron mobility in acceptor (μ_e) on the performance parameters shown in Fig. 7(a-c) resembles exactly the effect of hole mobility in donor (μ_h) shown in Fig. 8(a-c).

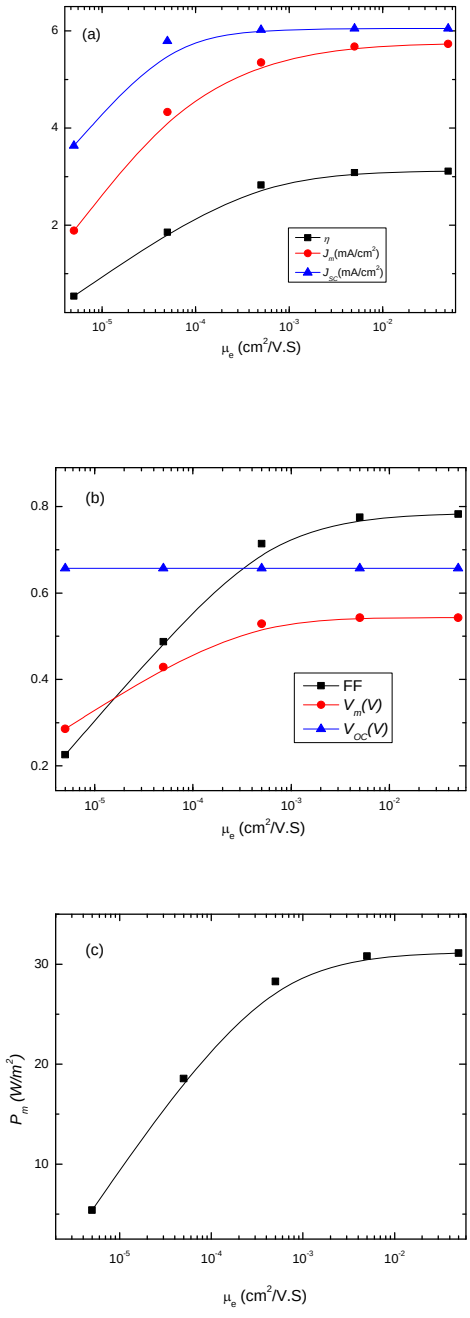

Fig. 7. (a) η, J_m, and J_{SC} versus μ_e, (b) FF, V_m and V_{OC} versus μ_e, (c) P_m versus μ_e.

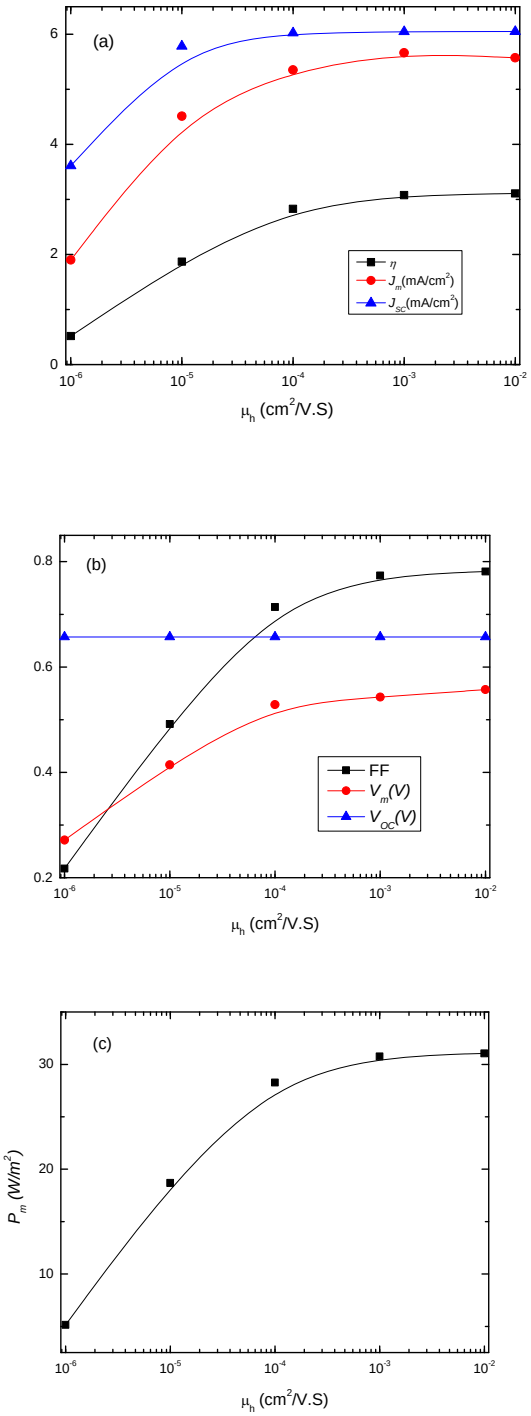

Fig. 8. (a) η, J_m, and J_{SC} versus μ_h, (b) FF, V_m and V_{OC} versus μ_h, (c) P_m versus μ_h.

The parameters η, J_m, and J_{SC} increase with increasing the exciton diffusion length in donor L_{ex}^D as shown in Fig. 9(a). In Fig. 9(b), while V_m remains constant V_{OC} increase from 0.62 to 0.66; therefore, FF degrades due to the enhancement of V_{OC} and J_{SC}. Fig. 9(c) shows the enhancement of P_m from 10 to 32 (W/m^2) as L_{ex}^D varies from 5 to 25 nm.

Comparing Fig. 9(a-c) with Fig. 10(a-c), L_{ex}^{A} has less effect on the performance parameters than L_{ex}^{D}. Moreover, the performance parameters depend linearly on L_{ex}^{A} but nonlinear on L_{ex}^{D}. In Fig. 10(a), η, J_m, and J_{SC} increase slightly with increasing L_{ex}^{A}. Fig. 10(b) shows that FF, V_{OC} and V_m are almost independent of L_{ex}^{A}.

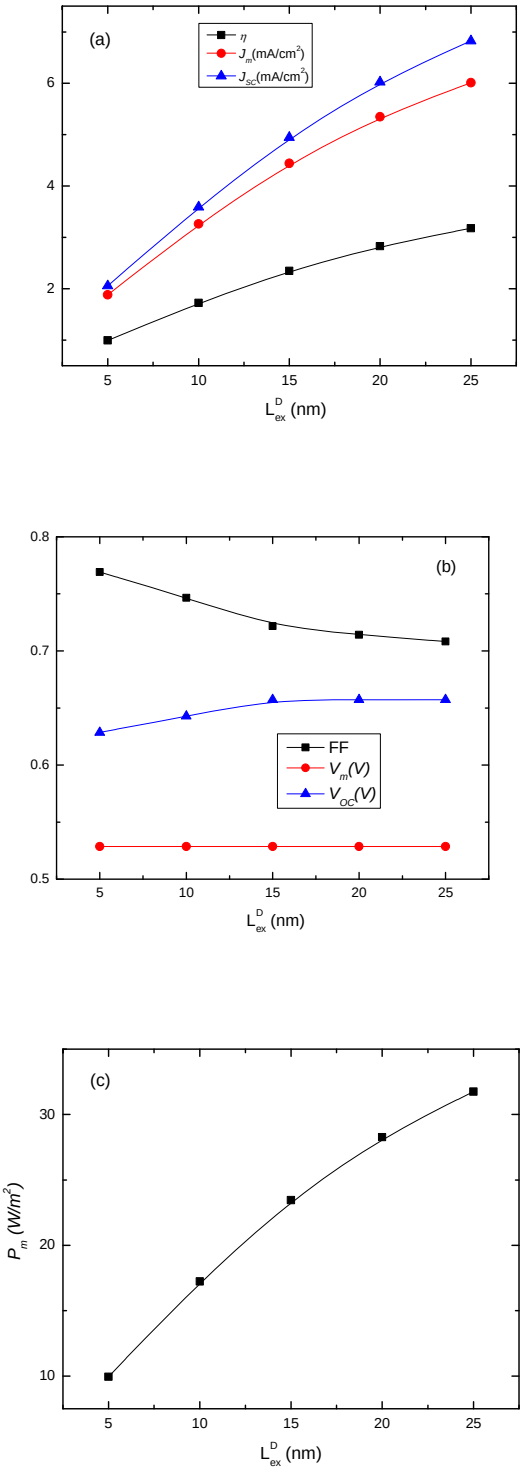

Fig. 9. (a) η, J_m, and J_{SC} versus L_{ex}^{D}, (b) FF, V_m and V_{OC} versus L_{ex}^{D}, (c) P_m versus L_{ex}^{D} .

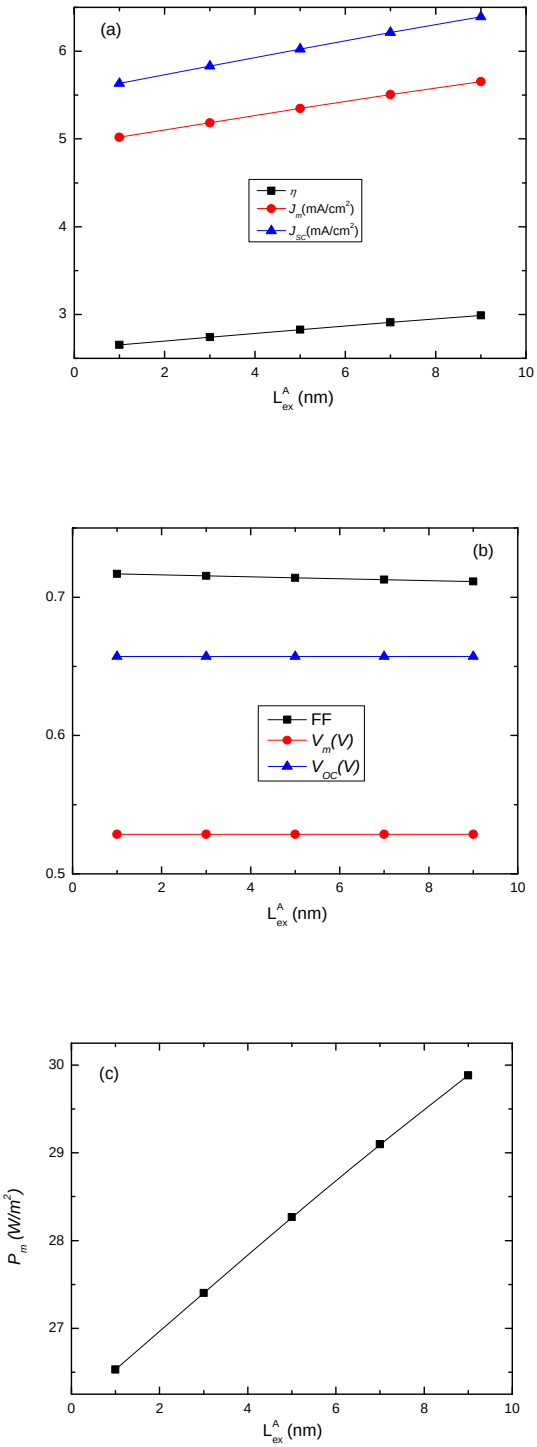

Fig. 10. (a) η, J_m, and J_{SC} versus L_{ex}^{A}, (b) FF, V_m and V_{OC} versus L_{ex}^{A}, (c) P_m versus L_{ex}^{A}.

All performance parameters degrade with increasing γ as shown in Fig. 11(a-c). However, the degrading of J_{SC} and J_m starts from $\gamma = 10^{-8}$ (cm^3/s).

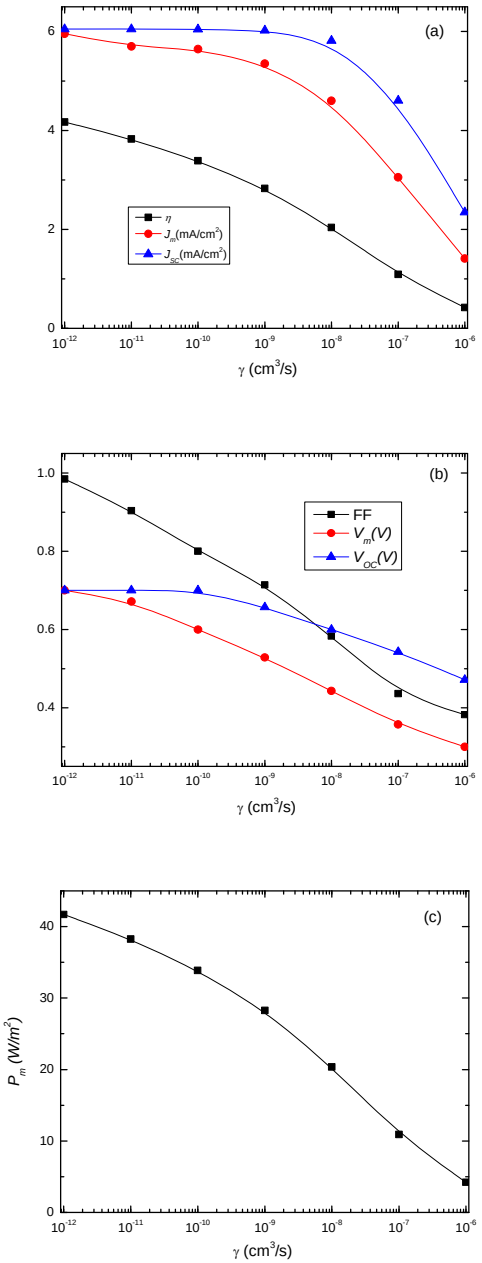

Fig. 11. (a) η, J_m, and J_{SC} versus γ, (b) FF, V_m and V_{OC} versus γ, (c) P_m versus γ.

3.3. Constant illumination effect on performance parameters

When OPV is subjected to constant illumination, with 2×10^{22} cm^{-3}s^{-1} photons absorption rate in the active layer, the obtained performance parameters are given in Table 2.

Table 2. OPV performance parameters for constant illumination.

η (%)	FF	P_m (W/m^2)	V_m	J_m (mA/cm^2)	V_{OC}	J_{SC}(mA/cm^2)
3.36	0.7	33.6	0.53	6.36	0.66	7.3

4. Conclusions, challenges and future perspectives

Simulation of ITO/P3HT/PCBM/Al OPV was carried out with the evaluation of the performance parameters; namely, efficiency, fill factor, open circuit voltage, short circuit current, maximum voltage, maximum current, and maximum power. Performance optimization of the device dimensions and material parameters are demonstrated too. Bilayer Heterojunction OPV is simulated because its analysis is simpler compared to complex random morphologies. Moreover, complex morphology devices can be geometrically transformed to equivalent planar structure, hence the analysis of planar hetero-junction devices is the root of the research on OPVs. The theoretical physics of these devices with a quantitative estimation of the effect of device dimensions and material parameters on the OPVs performance is achieved.

One of the challenges is the degradation of OPVs Efficiency. The degradation is attributed to four loss mechanisms [29]: optical, recombination, collection, and exciton losses. By far the greatest loss mechanism is exciton recombination at donor/acceptor interfaces resulting from mismatched energy levels between the two organic materials [29, 30, 23]. Another challenge for OPVs is that efficiencies decrease as the size of the cell increases. Increasing size of the cell results in higher sheet resistivity and greater defects in the organic films [23]. Electrochemical reactions at the electrodes could be another source of degradation. The back electrode in normal geometries is frequently aluminum, a metal that reacts with oxygen and water, resulting in cell degradation [31, 32]. For longer lifetime OPVs, the aluminum electrode should be replaced with a less reactive and high work function metal such as silver or gold. A buffer layer, either ZnO or TiOx nanoparticles, is commonly spin coated or printed on top of the ITO electrode in inverted cells which is more stable than PEDOT (the layer that covers ITO in normal devices) [23].

Organic/inorganic tandem cells could be the route to higher efficiency PVs. One of the shortcomings is the reliance on indium tin oxide (ITO) which is an expensive and brittle transparent conducting electrode. Replacing ITO with CVD graphene could eliminate one of the drawbacks associated with OPVs. Other promising emerging approach is quantum dots/organic hybrid OSCs featuring multi-electron generation upon a single incident photon; however, the present efficiency of this type of device is still low [33, 34].

The bandgap of P3HT is around 1.9 eV, limiting the absorbance to below a wavelength of 650 nm. At 650 nm only 22.4% of the photons of the solar spectrum under AM 1.5 conditions can be harvested; hence, decreasing the bandgap increases the total amount of photons that can be harvested from the solar spectrum. However, narrowing the polymeric bandgap will eventually result in degradation in power conversion efficiency. This is due to a decrease in open circuit voltage (V_{oc}). Therefore, a compromise should be done to utilize the optimal bandgap.

Due to the low exciton diffusion lengths of typical 1–10 nm in polymeric materials [35, 36], a simple bilayer structure will result in low efficiencies since only photons absorbed within this distance from the donor/acceptor interface will contribute to the device current [37]. A drastic increase in the generated photocurrent can be achieved by employing an interpenetrating network of donor and acceptor materials [38, 39]. When the interfaces between the P3HT layer and the PCBM layer and between the PCBM layer and the Al electrode were treated with methanol, the bilayer OPV showed significant enhancement of device performance with improved J_{SC}, *FF*, and efficiency [40].

This work helps to better understand the underlying relationship between the organic semiconductor materials and the OPVs performance and assist in further enhancement in the efficiency of OPVs. With better efficiency and longer lifetime, the OPVs will be competitive with their inorganic counterparts.

References

[1] M. A. Green, K. Emery, Y. Hishikawa, W. Warta, Prog. Photovoltaics **19**, 84 (2011).

[2] L. Dou, J. You, J. Yang, et al., Nature Photonics **6**, 180 (2012).

[3] M. A. Green, K. Emery, Y. Hishikawa et al., Prog. Photovoltaics **20,** 12 (2012).

[4] P. Peumans, Soichi Uchida, R. Stephen Forrest, Nature **425**, 158 (2003).

[5] C. Deibel, T. Strobel, V. Dyakonov, Adv. Mater. **22,** 4097 (2010).

[6] T.M. Clarke, J.R. Durrant, Chem. Rev. **110**, 6736 (2010).

[7] Yang Yang, Gang Li Editors, Progress in High-Efficient Solution Process Organic Photovoltaic Devices: Fundamentals, Materials, Devices and Fabrication, Springer (2015).

[8] X. L. Chen, B. H. Xu, J. M. Xue, Y. Zhao, C.C. Wei, J. Sun, Y. Wang, X. D. Zhang, X.H. Geng, Thin Solid Films **515**, 3753 (2007).

[9] V. Bhosle, J.T. Prater, Fan Yang, D. Burk, S.R. Forrest, J. Narayan, J. Appl. Phys. **102**, 023501 (2007).

[10] J. Owen, M.S. Som, K.H. Yoo, B.D. Ahnand, S.Y. Lee, Appl. Phys. Lett. **90**, 033512 (2007).

[11] Y. Yamamoto, K. Saito, K. Takahashi, M. Konagai, Sol. Energy Mater. Sol. Cells **65**, 125 (2001).

[12] S. Park, S.J. Tark, J.S. Lee, H. Lim, D. Kim, Sol. Energy Mater. Sol. Cells, **93**, 1020 (2009).

[13] O. Kluth, B. Rech, L. Hoben, S. Wieder, G. Schöpe, C. Beneking, H. Wagner, A. Löffl, Thin Solid Films **351**, 247 (1999).

[14] M.W. Rowell, M.A. Topinka, M.D. McGehee, H.J. Prall, G. Dennler, N.S. Sariciftci, L.B. Huand G. Gruner, Appl. Phys. Lett. **88**, 233506 (2006).

[15] G. Eda, Y.Y. Lin, S. Miller, C.W. Chen, W.F. Suand, M. Chhowalla, Appl. Phys. Lett. **92**, 233305 (2008).

[16] Y.H. Zhou, F.L. Zhang, K. Tvingstedt, S. Barrau, F.H. Li, W.J. Tianand O. Inganas, Appl. Phys. Lett. **92**, 233308 (2008).

[17] K. Tvingstedt, O.Inganäs, Adv. Mater. **19**, 2893 (2007).

[18] J.Y. Lee, S.T. Connor,Y.Cui, P. Peumans, Nano Lett. **8**, 689 (2008).

[19] B. O'Connor, C. Haughn, K.H. An, K.P. Pipe, M. Shtein, Appl. Phys. Lett. **93**, 223304 (2008).

[20] C. Guillen, J. Herrero, Sol. Energy Mater. Sol. Cells **92**, 938 (2008).

[21] A.C. Arango, L.R. Johnson, V.N. Bliznyuk, Z. Schlesinger, S.A. Carter, H.H Horhold, Adv. Mater. **12**, 1689 (2000).

[22] A.L. Ayzner, C.J. Tassone, S.H. Tolbert, B.J. Schwartz, The Journal of Physical Chemistry C **113**, 20050 (2009).

[23] C. Frederik Krebs, Polymeric Solar Cells: Materials, Design, Manufacture. DEStech Publications, Inc., Lancaster, Pennsylvania (2010).

[24] Peter Peumans, Aharon Yakimov, R. Stephen Forrest, Journal of Applied Physics **93**, 3693 (2003).

[25] L.A.A. Pettersson, L.S. Roman, O. Inganas, Journal of Applied Physics **86**, 487 (1999).

[26] H. Hoppe, N.S. Sariciftci, D. Meissner, Molecular Crystals and Liquid Crystals **385**, 113 (2011).

[27] V.S. Gevaerts, L.J.A. Koster, M.M. Wienk, R.A.J. Janssen, ACS Appl. Mater. Interfaces **3**, 3252 (2011).

[28] A.D. Rakic, Applied Optics **34**, 4755 (1995).

[29] Thomas Kirchartz, Kurt Taretto, Uwe Rau, J. Phys. Chem. **113**, 17958 (2009).

[30] E. Klimov, W. Li, X. Yang, G.G. Homann, J. Loos, Macromolecules **39**, 4493 (2006).

[31] M. Glattharr, M. Riede, N. Keegan, K. Sylvester-Hvid, B. Zimmermann, M. Niggemann, A. Hinsch, A. Gombert, Solar Energy Materials and Solar Cells **91**, 390 (2007).

[32] Christopher E. Petoukhoff, Divya K. Vijapurapu, Deirdre M. O'Carroll, Solar Energy Materials and Solar Cells **120**, 572 (2014).

[33] X. Gong, M. R. Robinson, J. C. Ostrowski, D. Moses, G. C. Bazan, A. J. Heeger, Adv. Mater. **14**, 581 (2002).

[34] X. H. Yang, D. Neher, Appl. Phys. Lett. **84**, 2476 (2004).

[35] D.E. Markov, E. Amsterdam, P.W.M. Blom, A. B. Sieval, J.C. Hummelen, J. Phys. Chem. A **109**, 5266 (2005).

[36] D. E. Markov, C.Tanase, P. W. M. Blom, J. Wildeman, Phys. Rev. B. **72**, 045217 (2005).

[37] M. Granstrom, K. Petritsch, A.C. Arias, A. Lux, M.R. Andersson, R.H. Friend, Nature **395**, 257 (1998).

[38] J.J.M. Halls, C.A. Walsh, N.C. Greenham, E.A. Marseglia R.H. Friend, S.C. Moratti, A.B. Holmes, Nature **376**, 498 (1995).

[39] G. Yu, J. Gao, J.C. Wudl F. Hummelen, A.J. Heeger, Science **270**, 1789 (1995).

[40] Jihoon Lee, Yun Kyung Jung, Dal Yong Lee, Jae-Won Jang, Shinuk Cho, Semo Son, Junghyun Jeong, Sung Heum Park, Synthetic Metals **199**, 408 (2015).

*Coresponding author: elaasser@gmail.com, elaasser@sci.asu.edu.eg